# Comparison of Wall Boundary Conditions for Numerical Viscous Free Surface Flow Simulation

I. Robertson [a] S.J. Sherwin [a,*] J.M.R. Graham [a]

[a] *Department of Aeronautics, Imperial College London, South Kensington Campus, London, SW7 2AZ, U.K.*

**Abstract**

A spectral/$hp$ element code, incorporating a velocity-pressure formulation, is used to simulate free surface flows. Non-linear pressure and velocity boundary conditions are applied on the moving free surface, the tracking of which is facilitated by the implementation of an Arbitrary Lagrangian Eulerian (ALE) formulation. The derived algorithm is validated by comparing the numerical results evaluated here with an analytical method which predicts the damping of a freely sloshing, viscous fluid for a range of Reynolds number: $3 \leq \text{Re} \leq 3 \times 10^5$ where $\text{Re} = (gd)^{1/2} d/\nu$ and $g$, $d$ and $\nu$ are gravity, depth of fluid and kinematic viscosity respectively. The free surface wall contact point is investigated and a number of approximations to overcome the contradiction of a moving contact point and the wall no-slip condition are presented. The numerical procedure which utilises these approximations is tested against a linear, analytical method which predicts viscous diffusion in the vicinity of the containing walls for a freely sloshing fluid. It is found that the numerical results using the various formulated boundary conditions converge as the Reynolds number increases.

## 1 Introduction

A major application of numerical solutions of free surface flows is the evaluation of wave forces on offshore structures, where the accurate prediction of the loads placed on and subsequent motion of marine installations are of paramount importance when considering the structural parameters of the body. Traditionally the majority of work in this area has been based on potential theory which treats the flow as inviscid and irrotational. Though linear theory can accurately predict these

* Corresponding author.

forces for small wave amplitudes, for naturally occurring sea conditions fully non-linear calculations are essential. Boundary element methods have been extensively used to computationally simulate such free surface flows (Celebi et al., 1998; Ferrant, 1996), though recent understanding of the computational efficiency of these algorithms has shown that the finite element method is a competitive numerical technique when a large number of degrees of freedom is used to discretise the fluid domain (Cai et al., 1998; Wu & Eatock Taylor, 1994). The finite element method has therefore become popular when simulating unsteady, inviscid free surface flows (Cai et al., 1998; Wu et al., 1998; Robertson & Sherwin, 1999) and in many cases has been extended to the solution of viscous free surface flows (Warburton & Karniadakis, 1997; Ramaswamy & Kawahara, 1987; Ramaswamy, 1989; Huerta & Wing Kam, 1988; Robertson, 2000).

Generally viscous effects and free surface diffraction effects are not both important in the same problem for a practical offshore structure. Though, the addition of viscous effects is necessary for the flow scenarios below:

- Viscous damping of wave excited oscillations of offshore structures,
- Flow past a body at high Keulegan-Carpenter number where free surface effects are locally important,
- Wave generation of submerged and floating bodies where a mean flow component causes seperation,
- Damping of sloshing waves in a container.

A contentious aspect of the numerical evaluation of viscous free surface flows is the nature of the free surface contact point on a wall. Though the no-slip condition is a basic premise of fluid dynamics, the motion of a free surface contradicts this condition. It can be seen experimentally that the contact point of the free surface, whilst theoretically adhering to a no-slip condition, is in relative motion along the adjoining wall. The contact point is not identifiable with a fluid particle. Various models are available to overcome this contradiction, either of an analytical nature (Dussan, 1976; Miles, 1991) or based on empirical data (Ting & Perlin, 1995; Hocking, 1987; Young & Davis, 1987). In most cases the recommended boundary conditions are not suitable for implementation within a numerical code. The schemes based on empirical data are generally extremely complicated and are dependent on the evaluation of small scale quantities such as contact angle and surface tension variation. These effects are largely unimportant when considering most marine and offshore problems. In addition, the schemes are dependent on the type of material at the contact walls and specific experimental data has to be evaluated before a relevant boundary condition can be formulated. Therefore these schemes are not applicable to a generalised free surface numerical code.

The most widely used computational model is the no-shear force or friction free condition (Huerta & Wing Kam, 1988), which is referred to in this work as the slip condition. This boundary condition does not promote the generation of vorticity at free surface contact walls, where it is theorised that much of the dissipation of the

energy of the fluid occurs (Keulegan, 1959; Miles, 1967). Therefore this boundary condition does not give satisfactory results for many free surface flows where viscous dissipation is important.

The nature of the free surface, in terms of its shape and velocity, is also affected by the boundary conditions placed on the contact walls (Dussan, 1976). Therefore models which allow the free surface contact point to be in motion whilst also producing appreciable boundary layers on free surface contact walls are necessary to allow the full investigation of the free surface flow of a contained body of fluid or the flow past a surface piercing structure. To this end contact wall boundary conditions are formulated which adhere to the proviso of a moving contact point, whilst also promoting the generation of boundary layers at the contact wall. The theorised boundary conditions are seen as an engineering solution to the described problem and not a highly accurate physical model of the flow characteristics at the wall/free surface contact point.

The governing equations of viscous flow are solved by utilising the ALE formulation which allows the mesh points to move with a velocity different to that of the velocity of the fluid, whilst adhering to some constraints for free surface flow. This procedure alleviates the production of highly deformed elements which would affect the stability of the computations. The first application of the ALE formulation was used in conjunction with a finite difference scheme (Hirt et al., 1974) and has since been extensively utilised for free surface problems using the finite element method (Huerta & Wing Kam, 1988; Ramaswamy & Kawahara, 1987). Ho (Ho, 1995) developed an ALE approach to simulate free surface flow using a spectral element discretisation based on conforming quadrilaterals and this formulation has been extended by Warburton and Karniadakis (Warburton & Karniadakis, 1997) to hybrid discretisations incorporating triangular and tetrahedral elements (Sherwin & Karniadakis, 1995a,b), where the vorticity generation induced by a cylinder close to a free surface is investigated. This spectral/$hp$ element formulation ensures fast convergence rates, minimal diffusion and dispersion errors on deformed elements (Warburton & Karniadakis, 1997) and also allows the fluid domain to be discretised using an unstructured mesh (Sherwin, 1995). Therefore complex geometries such as surface piercing cylinders and submerged bodies can be incorporated into the computational domain. The benefits of the ALE and spectral/$hp$ element formulations have therefore been utilised in this work to generate solutions to unsteady free surface flows with viscosity.

In order to study the various flow effects of viscous fluids with a free surface, the problem of a free surface wave undergoing free oscillations is investigated. Free oscillations occur when the free surface of a fluid has an initial prescribed deformation or pressure distribution and is allowed to oscillate with gravity as the only external force. The fluid motion generated by these conditions is commonly known as sloshing. Sloshing has the benefit of allowing the investigation of important problems in free surface fluid dynamics, such as nonlinearities, generation of boundary

3

layers at the free surface and walls and the complex issue of the determination of the nature of the free surface contact point, to take place in a controlled environment and without the need for inflow and outflow boundary conditions.

Sloshing has many areas of engineering application. The motion of any floating vessel on the open sea is affected by the motion of the sea itself. If the wave induced oscillations of the vessel are of the same resonant frequency as any fluid containment system within it, the forces and moments resulting from the fluid motion will affect the dynamic behaviour of the entire vessel and also place large structural loads on the surrounding walls. Oil cargo ships and liquid natural gas carriers often have tank dimensions such that the high resonant sloshing frequencies are in the same range as the induced ship motions (Solaas, 1995), leading to violent sloshing motions and large impact loads. Conversely, water tanks with internal sloshing have been fitted to ships as motion damping devices.

Advances in space flight are dependent upon the understanding of the forces and moments produced by a sloshing liquid in a microgravity environment where viscous and free surface effects dominate the flow. Similarly sloshing effects on the dynamic stability of light aircraft have to be considered.

Sloshing also has applications on a larger scale, for example the fluid motion within a harbour or lake can be affected by tidal oscillations and earthquake disturbances. These motions become increasingly important when a dam is used to contain a large body of water which becomes excited due to earthquake activity or landslides. Not only are the impact loads on the dam important, but also the possibility of the fluid over-spilling.

This paper is comprised of four sections, the first of which is this introduction. Section 2 formulates the governing equations for a viscous fluid with a free surface, including non-linear free surface boundary conditions. Also included in this section is the boundary condition schemes which approximate a no-slip surface at the contact walls. This is followed by section 3 which contains the validated numerical results for sloshing of an unbounded viscous fluid and a comparison of bounded sloshing for the various applied wall boundary conditions. The final section contains the conclusions.

## 2 Governing equations for a viscous fluid with a free surface

The tank and fluid configuration can be seen in Fig. 1, where the fluid is considered to be contained within a rigid tank of length $l$ and depth $d$, the side walls are vertical and the floor is horizontal. A fixed frame of reference is defined as $Oxz$ where $z$ points vertically upwards. The undisturbed free surface of the fluid is described by $z = 0$ and the deformation of the free surface is denoted by $\zeta$ where $z = \zeta(x;t)$ and $t$ represents time. The flow of a viscous, incompressible fluid under the influence of

4

gravity is therefore governed by the continuity equation,

$$\nabla \cdot \mathbf{u} = 0 \ , \tag{1}$$

where $\mathbf{u}$ has components $\mathbf{u} = (u_x\,(x, z; t)\,, u_z\,(x, z; t))$, and by the ALE Navier-Stokes equation,

$$\left.\frac{\partial \mathbf{u}}{\partial t}\right|_{\mathbf{w}} + ((\mathbf{u} - \mathbf{w}) \cdot \nabla)\,\mathbf{u} = -\frac{\nabla p}{\rho} + \nu \nabla^2 \mathbf{u} + \mathbf{G} \ , \tag{2}$$

where $p\,(x, z; t)$ is the pressure, $\mathbf{G} = (0, -g)$, $g$ is the force of gravity per unit mass, $\nu$ is the kinematic viscosity, $\rho$ the density and $\mathbf{w} = (w_x\,(x, z; t)\,, w_z\,(x, z; t))$. The notation $\big|_{\mathbf{w}}$ denotes that the derivative is evaluated on the moving frame of reference of velocity $\mathbf{w}$. This is the standard Arbitrary Lagrangian Eulerian formulation used by many investigators to simulate free surface flow in stationary tanks (Warburton & Karniadakis, 1997; Ramaswamy & Kawahara, 1987; Ramaswamy, 1989; Huerta & Wing Kam, 1988; Robertson, 2000). The conditions placed on the boundary of the fluid will be discussed in section 2.1. For convenience the notation to denote the velocity of the frame of reference on which the time derivative is evaluated will be relaxed in subsequent discussions.

The computational code, $\mathcal{N}\varepsilon\kappa\mathcal{T}\alpha r$ -ALE (Beskok & Warburton, 2001; Warburton & Karniadakis, 1997), solves the governing incompressible ALE equations by spatially discretising the domain using spectral/$hp$ elements (Karniadakis & Sherwin, 1997). Using this method the expansion basis comprises a set of shape functions of increasing polynomial order, $P$. The main advantage of this method is an exponential decrease in the error as $P$ linearly increases for smooth functions.

A high order splitting method is implemented to temporally discretise the governing equations. The splitting scheme used has been extensively documented and tested (Karniadakis et al., 1991) and more recently mathematically investigated by Guermond and Shen (Guermond & Shen, 2003). A brief overview is given here.

The ALE governing equations (1) and (2) are temporally discretised and split into three sub-steps,

$$\hat{\mathbf{u}} - \sum_{q=0}^{Je-1} \alpha_q \mathbf{u}^{n-q} = \Delta t \left( \sum_{q=0}^{Je-1} \beta_q \mathbf{N}\left(\mathbf{u}^{n-q}, \mathbf{w}^{n-q}\right) + \mathbf{F}^{n+1} \right) \ , \tag{3}$$

$$\frac{\hat{\hat{\mathbf{u}}} - \hat{\mathbf{u}}}{\Delta t} = -\frac{1}{\rho} \nabla \bar{p}^{n+1} \ , \tag{4}$$

$$\frac{\gamma_0 \mathbf{u}^{n+1} - \hat{\hat{\mathbf{u}}}}{\Delta t} = \nu \mathbf{L}\left(\mathbf{u}^{n+1}\right) \ , \tag{5}$$

where the superscript index $n$ refers to the relevant value being at time level $t_n =$

$n\Delta t$, $Je$ is the order of the time integration and $\gamma_0$ and $\alpha_i$ are the stiffly stable time integration coefficients (Karniadakis et al., 1991). $\mathbf{N}$ represnts the nonlinear convection terms in the ALE Navier Stokes equations and $\mathbf{L}$ represents the linear, diffusive terms.

The time integration coefficients $\beta_q$ can be evaluated by utilising Taylor expansions to extrapolate an arbitrary function at time level $(n+1)\,\Delta t$, $f^{n+1}$, in terms of $f^{n-q}$ for $0 \le q < Je$. The values of the time integration coefficients, $\gamma_0$, $\alpha_q$ and $\beta_q$ are given in table 1 up to the third order.

The intermediate values of velocity are represented as $\hat{\mathbf{u}}$ and $\hat{\hat{\mathbf{u}}}$, where $\hat{\hat{\mathbf{u}}}$ is assumed to be incompressible such that,

$$\nabla \cdot \hat{\hat{\mathbf{u}}} = 0 \tag{6}$$

and by taking the divergence of (4) to form a Poisson equation, $\bar{p}$ is evaluated such that,

$$\nabla^2 \bar{p}^{n+1} = \rho \nabla \cdot \left( \frac{\hat{\mathbf{u}}}{\Delta t} \right) \ , \tag{7}$$

coupled with suitable boundary conditions. The pressure term $\bar{p}^{n+1} = p^{n+1}$ ensures that $\mathbf{u}^{n+1}$ is incompressible. Although the continuity equation is imposed directly on the intermediate solution $\hat{\hat{\mathbf{u}}}$ , the divergence free condition of the final solution $\mathbf{u}^{n+1}$ is enforced through the pressure Poisson equation and consistent boundary conditions.

After $\mathbf{u}^{n+1}$ has been obtained $\mathbf{w}^{n+1}$ is evaluated, where $\mathbf{w}$ is the velocity of the mesh points represented by $\mathbf{X}_w = \mathbf{X}_w\,(x, z; t)$ and

$$\frac{d\mathbf{X}_w}{dt} = \mathbf{w} \ . \tag{8}$$

The mesh velocity is arbitrary everywhere except on the free surface and can be evaluated from a Laplacian equation

$$\nabla^2 \mathbf{w} = 0 \ , \tag{9}$$

as is done here following Ho (Ho, 1995). More recent work (Lohner & Yang, 1996) has advocated using a variable coefficient within the Laplacian matrix to enhance smoothing and prevent sudden distortions. Though this was found to be unnecessary when simulating the flow scenarios in this paper. The free surface boundary condition on $\mathbf{w}$ is evaluated using the kinematic boundary condition and will be derived in section 2.1. The next step then begins by evaluating the mesh point locations using the stiffly stable time integration coefficients used previously (see Table 1);

$$\gamma_0 \mathbf{X}_w^{n+1} = \sum_{q=0}^{Je-1} \alpha_q \mathbf{X}_w^{n-q} + \Delta t \sum_{q=0}^{Je-1} \beta_q \mathbf{w}^{n-q} \ . \tag{10}$$

6

## 2.1  Boundary conditions

In the following sections the pressure and velocity boundary conditions are formulated for wall boundaries and the free surface. The wall boundaries are decomposed into walls in contact with the free surface, contact walls, and those walls which are fully submerged and therefore not in contact with the free surface. The fully submerged walls can subsequently be treated in a normal fashion by adhering to the no-slip boundary condition. As discussed above alternative, pseudo-noslip boundary conditions must be formulated for the free surface contact walls.

### 2.1.1  Wall boundary conditions

**Pressure boundary condition**

The pressure boundary condition on the walls for the high order splitting scheme is obtained by taking the contributions of the temporally discretised Navier-Stokes equation (2) in the normal direction and using vector calculus identities to enforce divergence (Orszag et al., 1986; Karniadakis et al., 1991). The pressure boundary condition is therefore,

$$
\frac{1}{\rho}\frac{\partial \bar{p}}{\partial n} = \mathbf{n} \cdot \left( -\frac{\partial \mathbf{u}}{\partial t}^{n+1} + \sum_{q=0}^{Je-1} \beta_q \mathbf{N}\left(\mathbf{u}^{n-q}, \mathbf{w}^{n-q}\right) \right.
$$
$$
\left. + \nu \sum_{q=0}^{Je-1} \beta_q \left( -\nabla \times (\nabla \times \mathbf{u})^{n-q} \right) + \mathbf{F}^{n+1} \right) . \tag{11}
$$

**Velocity Boundary Condition on Fully Submerged Walls**

The velocity boundary condition on walls not in contact with the free surface, generally the floor wall, is the no-slip condition and therefore for a fixed tank:

$$
u_x = 0 , \tag{12}
$$
$$
u_z = 0 . \tag{13}
$$

**Velocity Boundary Condition on Free Surface Contact Walls**

The velocity boundary condition specified on walls in contact with the free surface is not well posed due to the contradiction of the moving free surface and a no-slip condition on the bounding wall. Four alternative free surface contact wall boundary conditions have been adopted in the current work. They are then tested in the following sections for various flow scenarios and their effect on the fluid flow examined.

*'Slip' wall boundary condition*

The contact wall boundary problem has been overcome by many authors (Huerta & Wing Kam, 1988; Warburton & Karniadakis, 1997) by adopting a slip boundary condition on the free surface contact walls such that the non-permeability condition is maintained, whilst the tangential velocity is allowed to take a non-zero value by implementing a Neumann boundary condition at the wall. The resulting boundary conditions for the vertical side walls are,

$$u_x = 0 \; , \tag{14}$$

$$\frac{\partial u_z}{\partial x} = 0 \; . \tag{15}$$

These conditions relate to a zero shear force premise at the walls and therefore no production of vorticity at these walls.

*'Semi-slip' wall boundary condition*

The semi-slip boundary condition is formulated by following the ideas of Dussan (Dussan, 1976), who analytically studied the lowering of an infinitely long, inclined flat plate into a fluid. At the contact point, that is the point at which the free surface meets the plate, the fluid is allowed to slip and the no-slip boundary condition is approached with increasing distance from the contact point. The resulting fluid boundary conditions on the flat plate are,

$$\mathbf{u} \cdot \mathbf{n} = \mathbf{V_f} \cdot \mathbf{n} \; , \tag{16}$$

$$\mathbf{u} \cdot \mathbf{s} = U_n\left(r\right) \mathbf{V_f} \cdot \mathbf{s} \; , \tag{17}$$

where $\mathbf{V_f}$ is the velocity of the flat plate and $\mathbf{n}$ and $\mathbf{s}$ the unit normal and tangent to the plate respectively, $r$ is the distance along the flat-plate from the contact point and

$$U_n\left(r\right) = \frac{r^n}{1 + r^n} \; , \tag{18}$$

where $0 < n < \infty$ and therefore $\lim_{r \to \infty} U_n = 1$, resulting in the no-slip condition being reached at infinity.

In a similar manner a semi-slip condition is computationally implemented on the contact walls, denoted by $S'$, with $\Omega'$ representing the remainder of the boundary and interior, by regulating the velocity of the fluid depending on the distance from the contact point. This is achieved by modifying the values of the intermediate velocity, $\hat{u}$ where $\hat{u} = (\hat{u}_x, \hat{u}_z)$, at the vertical contact walls according to the arbitrary expression,

$$\hat{u}_z^{\dagger} = H\left(\hat{u}_z\right) = \hat{u}_z \left(\frac{z+d}{\zeta_w + d}\right)^2 \quad \text{on} \quad S' \,, \tag{19}$$

$$= \hat{u}_z \quad \text{on} \quad \Omega' \,, \tag{20}$$

where $\zeta_w = z(\pm\frac{l}{2}, t)$ is the displacement of the contact point on the wall. This function acts as a projection from a slip condition at the side walls to a semi-noslip condition. The three semi-discrete sub-steps (3-5) used to propagate the values of $\mathbf{u}$ and $\bar{p}$ are therefore modified to,

$$\hat{\mathbf{u}} - \sum_{q=0}^{Je-1} \alpha_q \mathbf{u}^{n-q} = \Delta t \left(\sum_{q=0}^{Je-1} \beta N\left(\mathbf{u}^{n-q}, \mathbf{w}^{n-q}\right) + \mathbf{F}^{n+1}\right) \,, \tag{21}$$

$$\begin{bmatrix} \hat{u}_x^{\dagger} \\ \hat{u}_z^{\dagger} \end{bmatrix} = \begin{bmatrix} \hat{u}_x \\ H\left(\hat{u}_z\right) \end{bmatrix} \tag{22}$$

$$\frac{\hat{\hat{\mathbf{u}}} - \hat{\mathbf{u}}^{\dagger}}{\Delta t} = -\frac{1}{\rho}\nabla\bar{p}^{n+1} \,, \tag{23}$$

$$\frac{\gamma_0 \mathbf{u}^{n+1} - \hat{\hat{\mathbf{u}}}}{\Delta t} = \nu \mathbf{L}\left(\mathbf{u}^{n+1}\right) \,, \tag{24}$$

and the pressure is evaluated by

$$\nabla^2 \bar{p}^{n+1} = \rho\nabla \cdot \left(\frac{\hat{\mathbf{u}}^{\dagger}}{\Delta t}\right). \tag{25}$$

The contact wall boundary conditions placed on the evaluation of $\mathbf{u}$ in equation (24) are the slip boundary conditions (14-15).

### 'Semi-noslip' wall boundary conditions

Another alternative is to place no-slip boundary conditions on some fraction of the wall and slip conditions on the remainder, with the slip conditions occupying the upper portion of the wall. An example is shown in Fig. 2 where the darker elements indicate a no-slip boundary condition on the wall and the lighter elements a slip boundary. The designated fraction of slip elements against no-slip elements is arbitrary and therefore user defined.

### 'Robin' wall boundary conditions

A similar method to the semi-noslip wall condition is the Robin boundary condition, where the no-slip boundary condition is enforced at some distance from the free-surface, whilst the slip condition is enforced on the free surface. In practice the Robin boundary condition is specified within the top element. Within the length of the boundary between the slip and no-slip condition the velocity is allowed to

9

"smoothly" vary in order to minimise instabilities. The condition within this slip-distance, $l_s$, is:

$$u_x = 0 \; , \tag{26}$$

$$\alpha \frac{\partial u_z}{\partial x} + \beta u_z = 0 \; , \tag{27}$$

where $\alpha = \alpha(z)$ and $\beta = \beta(z)$. $\alpha$ and $\beta$ can take any reasonable form, in the present work they are represented as polynomials:

$$\alpha = \left( \frac{z - z_s}{z_f - z_s} \right)^n \; , \tag{28}$$

$$\beta = 1 - \alpha \; , \tag{29}$$

where $z_s$ represents the vertical height of the start of the slip length, $z_f$ represents the free surface height and therefore $l_s = z_f - z_s$. The value of $n$ can take any positive value; a large value would equate to the dominance of the no-slip contribution to the Robin boundary condition. The variation of $\alpha$ and $\beta$ is shown in Fig. 3 for $n = 2$, which is the value used for all computations reported here. This choice of $n$ results in both $d\alpha/dz$ and $d\beta/dz$ being zero, thus ensuring a smooth transition from the no-slip condition to the mixed Robin condition.

Once again the designated fraction of slip elements against Robin elements is arbitrary and therefore user defined. The size of the slip elements will effect the computational results, though it will be shown the results converge as the element size is decreased.

### 2.1.2   Free surface boundary conditions

The pressure and velocity boundary conditions on the free surface are both formulated from the dynamic constraint of continuity of normal momentum flux across the free surface, whilst assuming negligible momentum on the air side and neglecting surface tension. The component of the stress tensor in the outward normal direction is therefore,

$$\sigma_{ij} n_j = 0 \; , \tag{30}$$

by substituting in the expression for the stress tensor the free surface dynamic condition becomes

$$-p n_i + \mu \left( \frac{\partial u_i}{\partial x_j} + \frac{\partial u_j}{\partial x_i} \right) n_j = 0 \; , \tag{31}$$

for zero atmospheric pressure. By resolving this condition in the direction normal and tangential to the free surface we can formulate pressure and velocity boundary conditions at the free surface.

10

**Free Surface Pressure Boundary Condition**

The normal component of the dynamic free surface boundary condition (31) gives a Dirichlet boundary condition for the pressure,

$$-p n_i n_i + \mu \left( \frac{\partial u_i}{\partial x_j} + \frac{\partial u_j}{\partial x_i} \right) n_j n_i = 0. \tag{32}$$

This condition enforces the balance between the externally applied stresses and the internal stresses. In two dimensions where $\mathbf{n} = (n_x, n_z)$ and $\mathbf{u} = (u_x, u_z)$ and neglecting surface tension

$$-p + 2\mu \left( \frac{\partial u_x}{\partial x} n_x^2 + \left( \frac{\partial u_x}{\partial z} + \frac{\partial u_z}{\partial x} \right) n_x n_z + \frac{\partial u_z}{\partial z} n_z^2 \right) = 0 . \tag{33}$$

Commonly this is rewritten by dividing through by $n_z^2$ and representing the pressure boundary condition in terms of the velocity and free surface gradients,

$$-p + \frac{2\mu}{1 + \left( \frac{\partial \zeta}{\partial x} \right)^2} \left( \frac{\partial u_x}{\partial x} \left( \frac{\partial \zeta}{\partial x} \right)^2 - \left( \frac{\partial u_x}{\partial z} \frac{\partial u_z}{\partial x} \right) \frac{\partial \zeta}{\partial x} + \frac{\partial u_z}{\partial z} \right) = 0 , \tag{34}$$

where $\frac{\partial \zeta}{\partial x} = -\frac{n_x}{n_z}$.

**Free Surface Velocity Boundary Condition**

The tangential component of equation (31) gives a Neumann boundary condition for the free surface. The tangential contribution to the dynamic free surface boundary condition is

$$\mu \left( \frac{\partial u_i}{\partial x_j} + \frac{\partial u_j}{\partial x_i} \right) n_j s_i = 0 , \tag{35}$$

where $\mathbf{s}$ is the unit tangent vector. By substituting $\mathbf{s} = (n_z, -n_x)$ the condition becomes,

$$2\frac{\partial u_x}{\partial x} n_x n_z + \left( \frac{\partial u_x}{\partial z} + \frac{\partial u_z}{\partial x} \right) n_z^2 - \left( \frac{\partial u_z}{\partial x} + \frac{\partial u_x}{\partial z} \right) n_x^2 - 2\frac{\partial u_z}{\partial z} n_z n_x = 0 . \tag{36}$$

The necessary Neumann boundary conditions for the velocity are not immediately obvious, though by rearranging equation (36) and using the continuity equation (1) two Neumann boundary conditions for the velocity can be formulated as,

$$\frac{\partial u_x}{\partial n} = -\frac{\partial u_x}{\partial x}n_x - \frac{\partial u_x}{\partial z}\frac{\partial \zeta}{\partial x}n_x - \frac{\partial u_z}{\partial x}\left(\frac{\partial \zeta}{\partial x}n_x + n_z\right) + 2\frac{\partial u_z}{\partial z}n_x \ , \qquad (37)$$

$$\frac{\partial u_z}{\partial n} = \frac{\partial u_x}{\partial x}\left(2\frac{\partial \zeta}{\partial x}\frac{1}{n_z} - n_z\right) + \frac{\partial u_x}{\partial z}n_x\left(\left(\frac{\partial \zeta}{\partial x}\right)^2 - 1\right)$$

$$+ \frac{\partial u_z}{\partial x}\left(\frac{\partial \zeta}{\partial x}\right)^2 n_x - 2\frac{\partial u_z}{\partial z}\frac{\partial \zeta}{\partial x}n_x \ . \qquad (38)$$

**Kinematic Boundary Condition**

The kinematic boundary condition in its most general form is

$$\mathbf{u} \cdot \mathbf{n} = \mathbf{w} \cdot \mathbf{n} \ , \qquad (39)$$

which simply states there is no normal flow of fluid over the free surface interface. We are not constrained however to move the mesh velocity $\mathbf{w}$ with the same tangential velocity as the fluid and so can arbitrarily fix one component of $\mathbf{w}$. To limit the distortion of elements and promote a stable solution we choose to specify $w_x = 0$ and so in two dimensions equation (39) can be written as,

$$u_x n_x + u_z n_z = w_z n_z \ . \qquad (40)$$

Dividing through by $n_z$ and recognising that $\frac{\partial \zeta}{\partial x} = -\frac{n_x}{n_z}$ we arrive at

$$u_z = w_z + u_x\frac{\partial \zeta}{\partial x} \ . \qquad (41)$$

$w_z$ can be used as a Dirichlet boundary condition when evaluating the velocity $\mathbf{w}$ in the interior of the fluid using equation (9). The choice of the Dirichlet boundary conditions for $w_z$ on the side and floor walls is arbitrary and can be linearly evaluated from the velocity of the free surface at the wall. For example at the wall $x = -\frac{l}{2}$,

$$w_z\left(-\tfrac{l}{2}, z; t\right) = \frac{z + d}{\zeta_w + d}w_z\left(-\tfrac{l}{2}, \zeta_w; t\right) \ , \qquad (42)$$

where $\zeta_w = \zeta\left(\pm\tfrac{l}{2}; t\right)$.

## 3  Numerical Results

### 3.1  Validation of unbounded sloshing

Various analytical methods exist to determine the rate of decay rate of a gravity bounded wave given some initial displacement (Landau & Lifschitz, 1959; Wu et al.,

2001). In this section results evaluated using a method derived by Landau and Lifshitz (Landau & Lifschitz, 1959) to theoretically predict damping rates for a freely sloshing fluid are compared with those produced by the numerical algorithm. Landau and Lifshitz (Landau & Lifschitz, 1959) obtain an exact solution to the linear free surface governing equations for a fluid with infinite depth by utilising diffusion length characteristics. The solution can be approximated to produce decay rates and frequencies for high or low Reynolds number flow. Here the solution is solved exactly and is therefore applicable for flow at all Reynolds number, though the amplitude to wavelength ratio of the wave must be small to ensure linearity. The Reynolds number is defined by

$$\mathrm{Re} = \frac{(gd)^{1/2} d}{\nu} \, , \tag{43}$$

where $(gd)^{1/2}$ is the characteristic velocity and $d$ the characteristic length. All physical quantities are therefore non-dimensionalised by utilising this characteristic velocity and length. The decay rate, $\alpha$, is defined by,

$$a = a_0 e^{-\alpha t}, \tag{44}$$

where $a$ is the amplitude of the wave, $a_0$ is the initial amplitude and t represents time.

To eliminate the necessity to consider the influence of the boundary condition and the contact point of the free surface on the fixed vertical walls, a periodic domain is utilised such that the values of the prime variables on the left hand side of the domain are identical to those on the right hand side. This has the benefit of allowing the decay rate due to the free surface boundary layer to be isolated and evaluated, though there is a minimal contribution to the decay from the floor wall.

Before the comparison is given, the temporal and spatial convergence of the solution must be proved in order for the results to be considered valid. This is done by conducting the same experiment for various temporal and spatial discretisations. The fluid is initially at rest within a periodic domain of size $l = 2$, with an initial free surface displacement described by,

$$\zeta\left(x;0\right) = -a_0 \cos\left(kx\right), \tag{45}$$

where $k = 2\pi/l$ and $a_0 = 0.005$ thus ensuring a linear wave. The mesh used contains 100 quadrilateral elements and is shown in Fig. 4 at its initial displacement. The elements are smaller at the surface and floor to capture the boundary layer adequately, whilst relatively large elements occur in the body of the mesh due to the small velocity gradient present in this area.

The Reynolds number of the test case is 110.736. Fig. 5(a) shows the time history of the free surface at $x = 1/2$ for decreasing values of $\Delta\tau$. It can be seen from the graph that convergence in time is satisfied as the results are nearly identical

13

when using $\tau = 4.429 \times 10^{-3}$ and $\tau = 2.215 \times 10^{-3}$ . Fig. 5(b) shows the time history of the free surface for increasing values of $p$, rapid convergence in $p$ is achieved. For values of $P = 5$, $P = 7$ and $P = 9$ the results are indistinguishable.

The comparison with the analytical results is for a case where the fluid is initially at rest within a periodic domain of size $l = 0.2$, with an initial free surface displacement as described by equation (45) $k = 2\pi/l$ and $a_0 = 0.0005$. These parameters ensure a linear wave with minimal contribution to the damping of the motion from the floor wall. The numerical grid comprises 100 quadrilateral elements and is similar to that shown in Fig. 6, though the mesh used for this experiments has a depth many times the width of the domain. The computations were performed using a polynomial expansion basis of order 5. The numerical experiment was conducted over a range of Reynolds number and the displacement time history of the waves are shown in Fig. 7 for the point $x = -l/2$ with the analytical decay rate also shown. The good comparison between the analytical and computational decay rates can be seen in Table 2.

## 3.2 Comparison of contact wall boundary conditions

To be viable numerical schemes all the presented contact wall boundary conditions must spatially and temporally converge. This convergence is proved in the following sections.

### 3.2.1 Temporal and spatial convergence

Fig. 8 contains time-histories of the displacement of the free surface for a sloshing fluid at $x = -1/2$ for each implemented boundary condition and varying temporal increments. Again the fluid is initially at rest with a sinusoidally prescribed deformation such that,

$$\zeta(x; 0) = -a_0 \sin(kx) \ . \tag{46}$$

The governing parameters of the flow are $k = \pi/l$, $a_0 = 0.02$, $l = 2$ and Re = 3132 and an expansion basis of order 5 was used. The computational mesh is comprised of 100 elements and can be seen in Fig. 6. The slip length $l_s$ used with the seminoslip and Robin boundary conditions is $d/32$. The time increment is decreased and temporal convergence is shown both in the time-histories in Fig. 8 and also in the error estimates in table 3. The error shown is the rms error, $E_{\mathrm{rms}}$ where

$$E_{\mathrm{rms}} = \left( \sum_{i=1}^{N} \frac{(u_i^e - u_i^a)^2}{N} \right)^{1/2} \ , \tag{47}$$

and $N$ denotes the number of sample points, $u^e$ and $u^a$ are the exact and approximate solution respectively known at $N$ discreet points. As no exact solution exists, the

most accurate numerical solution is used in its place. For the temporal and spatial convergence investigations $u_e$ is evaluated for $\Delta t = 5 \times 10^{-4}$ and $P = 7$ respectively.

Spectral convergence is proved in a similar manner to temporal convergence. As $P$ is increased the time histories converge as shown in Fig. 9 and table 4.

In order for the contact wall boundary conditions with a user defined slip length to be viable and reliable computational schemes the numerical results should converge as the slip length is decreased. This convergence is illustrated by the displacement time histories in Fig. 10 where the difference between the motion of the fluid decreases as the slip length decreases. This decrease can also be seen in the error estimates in table 5 where the most accurate solution, $u^e$, is attributed to $l_s = d/64$.

### 3.2.2 Comparison of analytical and numerical results for a fully bounded fluid

The decay rate of a sloshing fluid undergoing free surface standing wave motion has been evaluated numerically and compared with an analytical formulation derived by Keulegan (Keulegan, 1959). The analytical derivation was undertaken by presuming the energy dissipation due to the introduction of side and bottom walls occurs within the vorticity layers generated at these walls. The velocity within the main body of the fluid is evaluated using the well known potential formulation (Lamb, 1975) and close to the wall by boundary layer techniques incorporating the characteristic diffusion length. This analytical result was found to be in good agreement with physical experiments performed by Keulegan (Keulegan, 1959) when the Reynolds number is high, Re $\approx 1 \times 10^6$, and the main agent for diffusion is the generation of vorticity at the side and floor walls.

Fig. 11 contains displacement time-histories of a free surface at $x = -l/2$ with initial conditions given by equation (46) and $k = \pi/l$, $a_0 = 0.02$, $l = 2$, $312 \le$ Re $\le 31321$ and $P = 5$ using the various boundary conditions. The analytical decay rate of Keulegan (Keulegan, 1959) is also shown. When using the slip boundary condition the decay rate is too shallow due to the exclusion of vorticity generation at the side walls. Fig. 11 also illustrates that the results when the other three boundary conditions are implemented encouragingly converge as the Reynolds number increases.

Table 6 contains the numerical and analytical decay rates where a good comparison can be seen between the numerical and analytical results for the two highest Reynolds numbers where the analytical formulation is valid.

### 3.2.3 Vorticity generation and contact point behaviour

Vorticity generation at the side walls is one of the most important functions of the applied boundary conditions when considering the damping of an oscillating

15

fluid or moving body within a fluid. Vorticity contours for a sloshing fluid are shown in Fig. 12 where $t = 9.40$, $k = \pi/l$, $l = 2$ and Re $= 3123$. As expected vorticity is generated at the side walls when using the semi-slip, semi-noslip and Robin boundary conditions. The vorticity generated there is greater than that produced by the floor wall due to the exponential increase in velocity with height. The velocity gradient at the side walls leads to the free surface undergoing a relatively large deformation at the wall contact point, shown in Fig. 13. The free surface at the wall is trailing the main body of the fluid due to the implementation of the pseudo-noslip boundary conditions. As no vorticity is generated at the side walls when using the slip condition there is no deformation at the wall contact point.

## 4  Conclusion

The formulated viscous, free surface numerical code has been shown to be highly accurate when compared to analytical decay rates for an unbounded sloshing wave. Various contact wall boundary conditions have been presented and evaluated by comparison to an analytical derivation to calculate the damping of a fully bounded sloshing fluid. Where the analytical results are valid, the comparison with the present numerical results has been found to be favourable. Important applied shear forces identified by the semi-noslip boundary condition, are not captured by the slip boundary condition. Therefore to accurately simulate industrial fluid structure interaction scenarios a pseudo-noslip boundary condition, such as those presented here, is necessary.

**Acknowledgements**

# References

Beskok, A., Warburton, T., 2001. An unstructured *hp* finite-element scheme for fluid flow and heat transfer in moving domains. Journal of Computational Physics 174, 492–509.

Cai, X., Langtangen, H., Neilsen, B., Tveito, A., 1998. A finite element method for fully nonlinear water waves. Journal of Computational Physics 143, 544–568.

Celebi, M., Kim, M., Beck, R., 1998. Fully nonlinear three-dimensional numerical wave tank simulation. Journal of Ship Research 42, 33–45.

Dussan, E., 1976. The moving contact line: the slip boundary condition. Journal of Fluid Mechanics 77 (4), 665–684.

Ferrant, P., 1996. Simulation of strongly nonlinear wave generation and wave-body interactions using a 3d mel model. In: 21st Symposium on Naval Hydrodynaimcs. pp. 226–241.

Guermond, J., Shen, J., 2003. Velocity-correction projection methods for incompressible flows. SIAM J. Numer. Anal. 41, 112.

Hirt, C., Amsden, A., Cook, H., 1974. An arbitrary lagragian-eulerian computing method for all flow speeds. Journal of Computational Physics 14, 227–253.

Ho, L.-W., 1995. A legrende spectral element method for simulation of incompressible unsteady free-surface flows. Ph.D. thesis, Trondheim University.

Hocking, L., 1987. Waves produced by a vertically oscillating plate. Journal of Fluid Mechanics 179, 267–281.

Huerta, A., Wing Kam, L., 1988. Viscous flow with large free surface motion. Computer Methods in Applied Mechanics and Engineering 69, 277–324.

Karniadakis, G., Israeli, M., Orszag, S., 1991. High-order splitting methods for the incompressible navier-stokes equations. Journal of Computational Physics 97, 414–443.

Karniadakis, G., Sherwin, S., 1997. Spectral/hp element methods for CFD. Oxford University Press.

Keulegan, G., 1959. Energy dissipation in standing waves in rectangular basins. Journal of Fluid Mechanics 6, 33–50.

Lamb, H., 1975. Hydrodynamics, 6th Edition. Cambridge University Press.

Landau, L., Lifschitz, E., 1959. Fluid mechanics. Pergamon Press.

Lohner, R., Yang, C., 1996. Improved ale mesh velocities for moving bodies. Comm. Num. Meth. Eng. Phys. 12, 599–608.

Miles, J., 1967. Surface-wave damping in closed basins. Proc. Roy. Soc. Lond. Ser. A 297, 459–475.

Miles, J., 1991. Wave motion in a viscous fluid of variable depth. Journal of Fluid Mechanics 223, 47–55.

Orszag, S., Israeli, M., Deville, M., 1986. Boundary conditions for incompressible flows. J. Sci. Comput. 1, 75–87.

Ramaswamy, B., 1989. Numerical simulation of viscous free surafce flow. Journal of Computational Physics 90, 659–670.

Ramaswamy, B., Kawahara, M., 1987. Arbitrary lagragian-eulerian finite element method for unsteady, convective, incompressible viscous free surface flow. In:

in Fluids, F. E. (Ed.), Gallagher, RH and Glowinski, R and Gresho, PM and Oden, JT and Zienkiewicz, OC. Vol. 7. John Wiley and Sons, pp. 65–87.

Robertson, I., 2000. Free surface flow simulations using high order algorithms. Ph.D. thesis, Imperial College London.

Robertson, I., Sherwin, S., 1999. Free-surface flow simulations using $hp$/spectral elements. J. Comp. Phys 155, 26–53.

Sherwin, S., 1995. Triangular and tetrahedral spectral/$hp$ finite element methods for fluid dynamics. Ph.D. thesis, Princeton University, Department of Mechanical and Aerospace Engineering.

Sherwin, S., Karniadakis, G., 1995a. Tetrahedral $hp$ finite elements: algorithms and flow simulations. International Journal of Numerical Methods in Engineering 38, 37–75.

Sherwin, S., Karniadakis, G., 1995b. A triangular spectral element method; applications to the incompressible navier-stokes equations. Computer methods in applied mechanics and engineering 123, 189–229.

Solaas, F., 1995. Analytical and numerical studies of sloshing in tanks. Ph.D. thesis, Trondheim University.

Ting, C., Perlin, M., 1995. Boundary conditions in the vicinity of the contact line at a vertically oscillating upright plate: an experimental investigation. Journal of Fluid Mechanics 295, 263–300.

Warburton, T., Karniadakis, G., 1997. Spectral simulations of flow past a cylinder close to a free surface. ASME FEDSM97-3389 .

Wu, G., Eatock Taylor, R., 1994. Finite element analysis of two-dimensional nonlinear transient water waves. Applied Ocean Research 16, 363–372.

Wu, G., Eatock Taylor, R., Greaves, D., 2001. The effect of viscosity on the transient free-surface waves in two-dimensional tank. Journal of Engineering Mathematics 40, 77–90.

Wu, G., Ma, Q., Eatock Taylor, R., 1998. Numerical simulation of sloshing waves in a 3d tank based on a finite element method. Applied Ocean Research 20 (6), 337–355.

Young, G., Davis, S., 1987. A plate oscillating across a liquid interface: effect of contact angle hysteresis. Journal of Fluid Mechanics 174, 327–356.
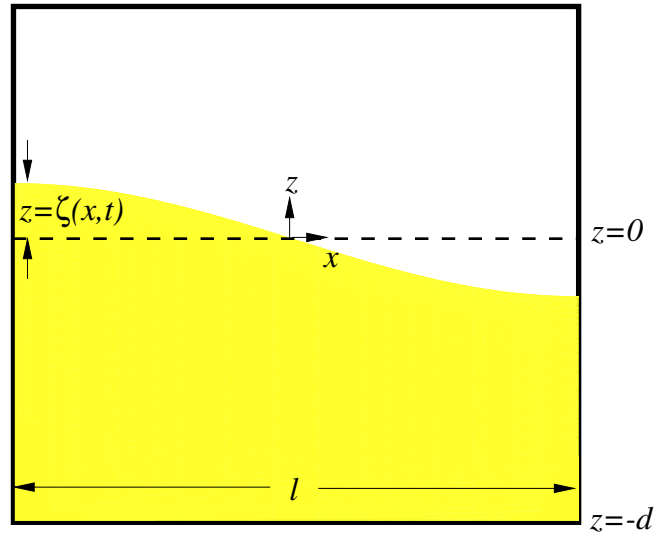
Fig. 1. Definition of frame of reference and wall boundary conditions for contained free surface system
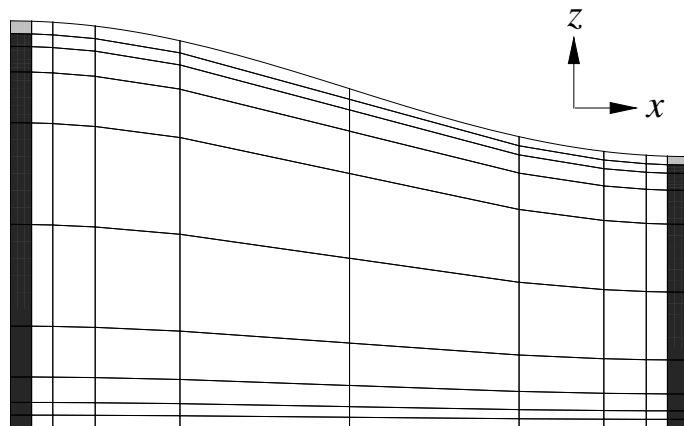


Fig. 2. Placement of slip/no-slip boundary conditions for a 'no-slip' wall boundary condition
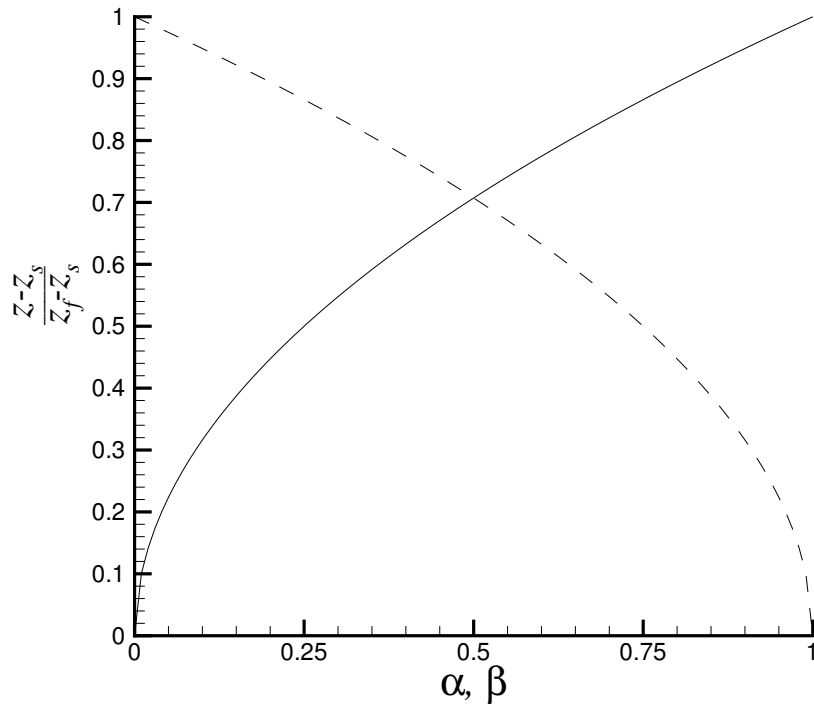
Fig. 3. Variation of $\alpha$ and $\beta$ as $z$ increases: ——————— $\alpha$, — — — — — — $\beta$
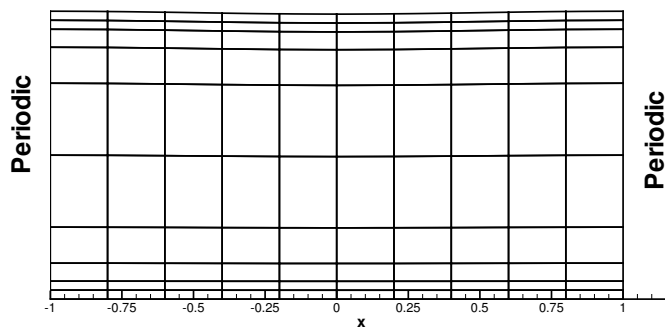


Fig. 4. Mesh used for small amplitude sloshing
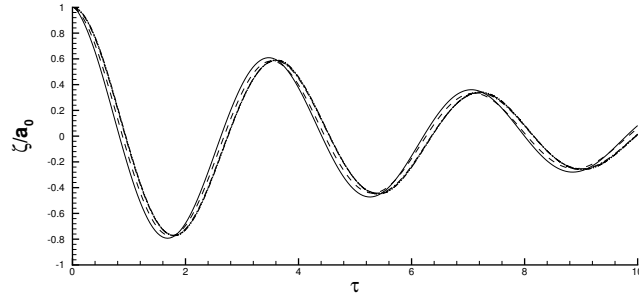
(a) Temporal convergence for decreasing time-step: ——
—— $\Delta\tau = 4.429 \times 10^{-2}$, $- - - - - \Delta\tau = 2.215 \times$
$10^{-2}$, $\cdot - \cdot - \cdot - \Delta\tau = 4.429 \times 10^{-3}$, $\cdots\cdots \Delta\tau =$
$2.215 \times 10^{-3}$, $- \cdot\cdot - \cdot\cdot - \cdot\cdot \Delta\tau = 4.429 \times 10^{-4}$.
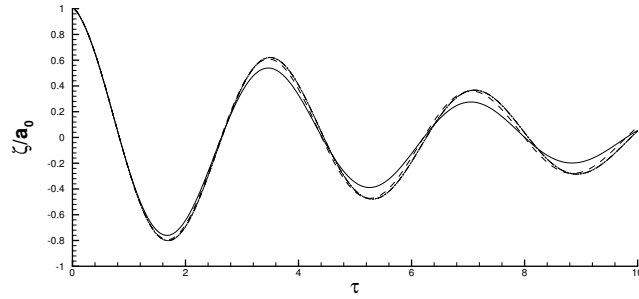


(b) Spatial convergence for increasing polynomial order :
———— $p = 1$, $- - - - - p = 3$, $\cdot - \cdot - \cdot - P =$
5, $\cdots\cdots P = 7$, $- \cdot\cdot - \cdot\cdot - \cdot\cdot P = 9$.

Fig. 5. Time history of free surface at $x = -l/2$ showing 5(a) temporal convergence and 5(b) spatial convergence
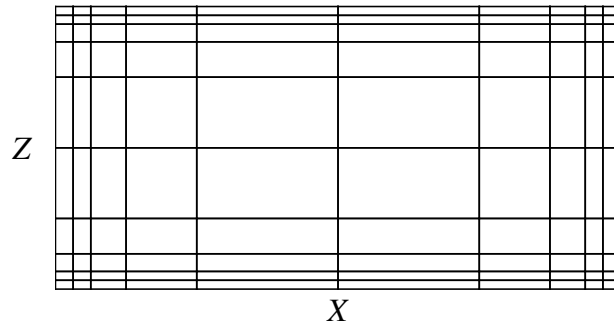


Fig. 6. Mesh configuration for wall boundary condition numerical simulations
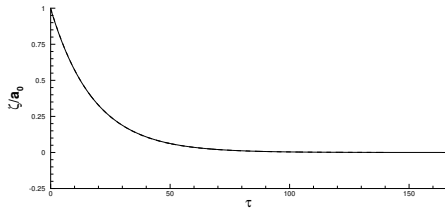
(a) Re = 3.50178
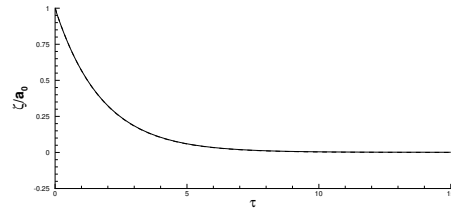
(b) Re = 35.0178
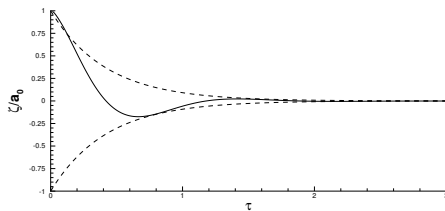
(c) Re = 350.178
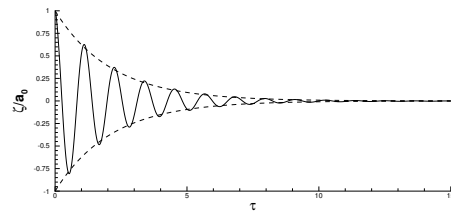
(d) Re = 3501.78
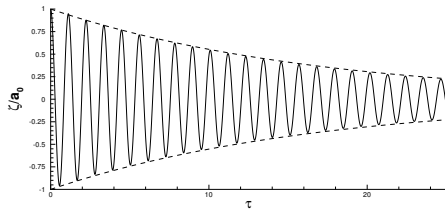
(e) Re = 35017.8
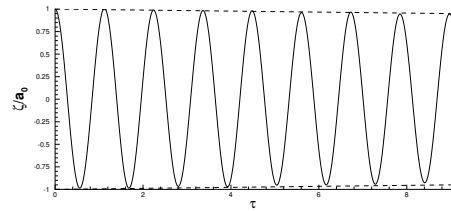
(f) Re = 350178

Fig. 7. Time history of free surface at $x = -l/2$ for $l = 0.2$ with increasing Reynolds number with predicted decay rate as dashed line.
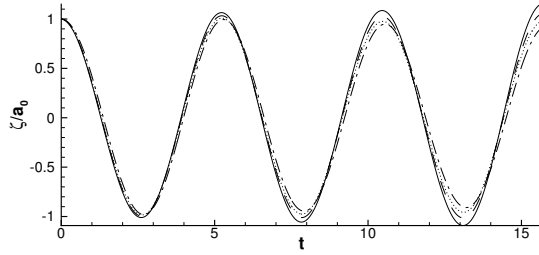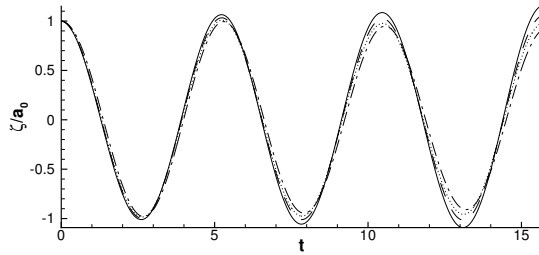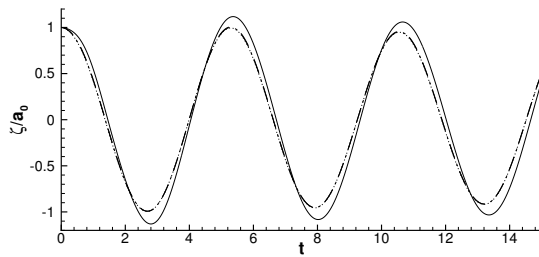
22

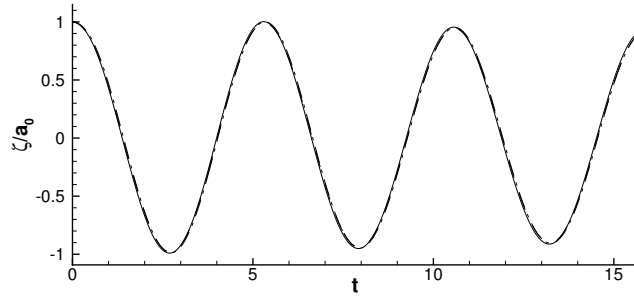(a) Slip boundary condition



(b) Semi-slip boundary condition
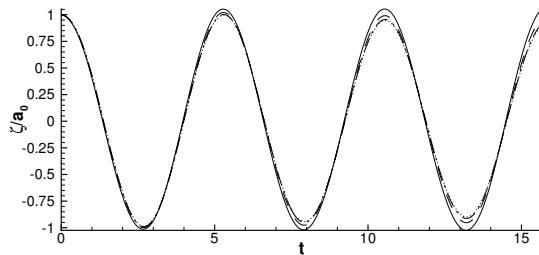


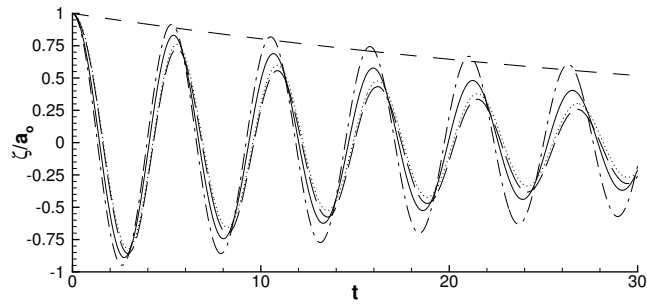(c) Semi-noslip boundary condition
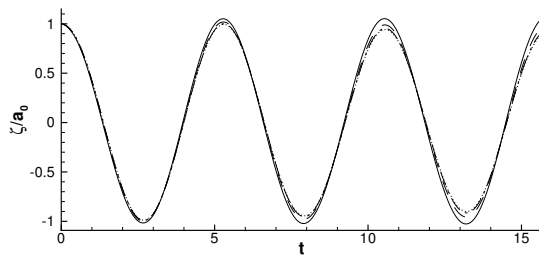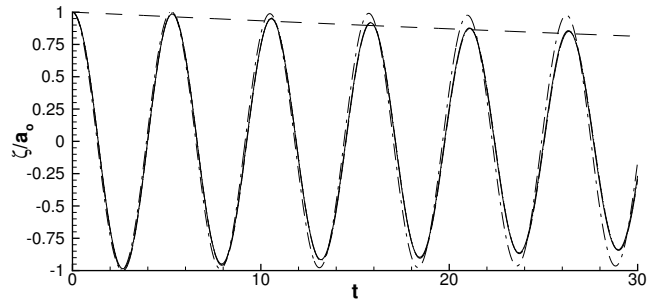


(d) Robin boundary condition

Fig. 8. Time history of free surface displacement for all wall boundary conditions showing temporal convergence: ——— $\Delta t = 1.57 \times 10^{-2}$, $- - - -$ $\Delta t = 7.83 \times 10^{-3}$, $- \cdot - \cdot - \cdot -\cdot$ $\Delta t = 3.13 \times 10^{-3}$ and $\cdots\cdots$ $\Delta t = 1.56 \times 10^{-3}$
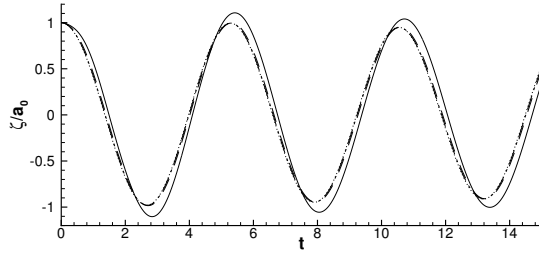
23

(a) Slip boundary condition
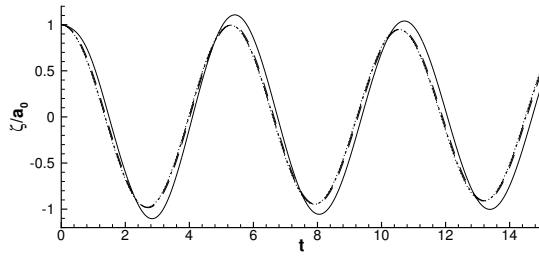


(b) Semi-slip boundary condition
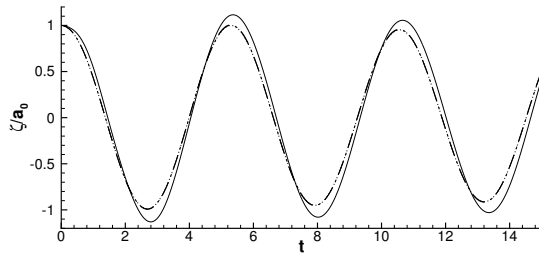


(c) Semi-noslip boundary condition



(d) Robin boundary condition
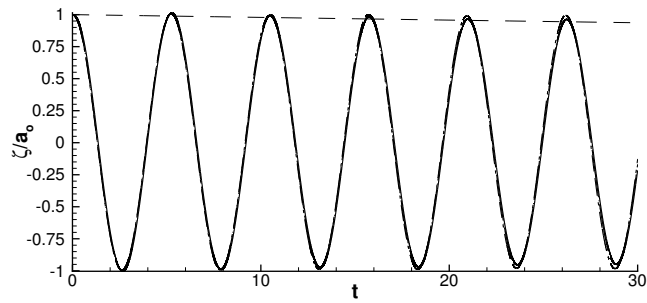
Fig. 9. Time history of free surface displacement for all wall boundary conditions showing spectral convergence:————— $P = 1$, $----$ $P = 3$, $-\cdot-\cdot-\cdot-\cdot$ $P = 5$ and $\cdots\cdots$ $P = 7$

(a) Semi-slip boundary condition
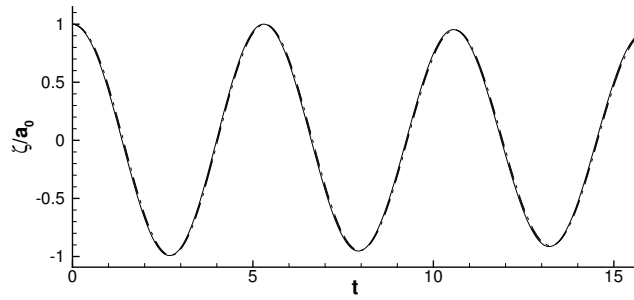


(b) Robin boundary condition

Fig. 10. Time history of free surface displacement for all wall boundary conditions showing slip length convergence: ——— $l_s = d/32$, $----$ $l_s = d/48$, $-\cdot-\cdot-\cdot-$ $l_s = d/64$
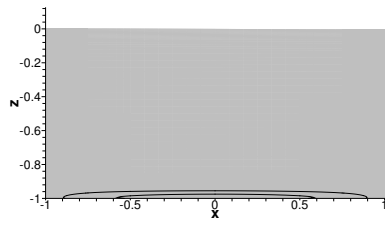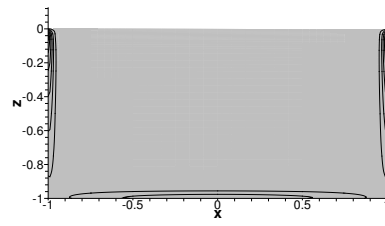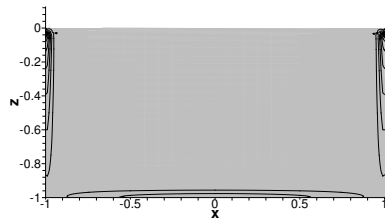
(a) Re = 313



(b) Re = 3132



(c) Re = 31321

Fig. 11. Time history of free surface at $x = -l/2$:– – – – Analytical decay rate, – · – · – · – Slip boundary condition, ——————— Semi-slip boundary condition, · · · · · · · Semi-noslip boundary condition, — — — Robin boundary condition

(a) Slip Boundary Condition



(b) Semi-slip Boundary Condition



(c) Semi-noslip Boundary Condition



(d) Robin Boundary Condition

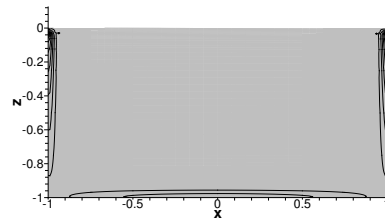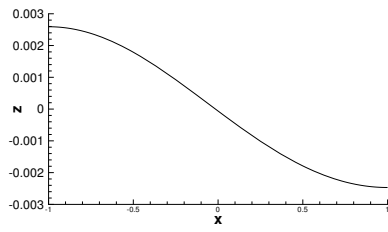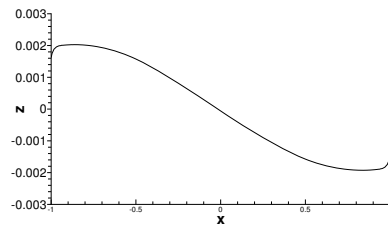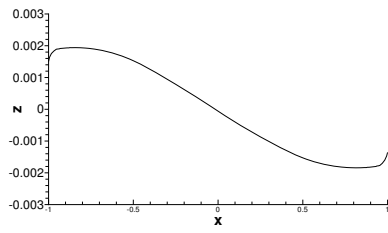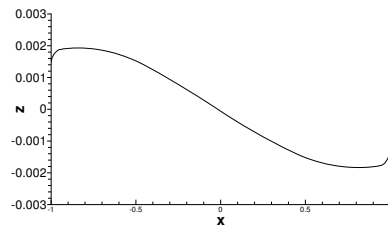Fig. 12. Vorticity contours at $t = 9.40$ for a fully bounded sloshing fluid

(a) Slip Boundary Condition

(b) Semi-slip Boundary Condition

(c) Semi-noslip Boundary Condition

(d) Robin Boundary Condition

Fig. 13. Free surface profile at $t = 9.40$ for a fully bounded sloshing fluid

| coefficient | $1^{st}$ Order | $2^{nd}$ Order | $3^{rd}$ Order |
|:---:|:---:|:---:|:---:|
| $\gamma_0$ | 1 | 3/2 | 11/6 |
| $\alpha_0$ | 1 | 2 | 3 |
| $\alpha_1$ | 0 | −1/2 | −3/2 |
| $\alpha_2$ | 0 | 0 | −1/3 |
| $\beta_0$ | 1 | 2 | 3 |
| $\beta_1$ | 0 | −1 | −3 |
| $\beta_2$ | 0 | 0 | 1 |

Table 1
Time integration coefficients for a high-order splitting scheme to solve the Navier-Stokes equations

| Test Case | Re | $\alpha_p$ | $\alpha_c$ | $\alpha_c/\alpha_p$ |
|:---:|:---:|:---:|:---:|:---:|
| A | 3.50178 | $5.57409 \times 10^{-2}$ | $5.59406 \times 10^{-2}$ | 1.00358 |
| B | 35.0178 | $5.65876 \times 10^{-1}$ | $5.62732 \times 10^{-1}$ | 0.994444 |
| C | 350.178 | 2.38943 | 2.41594 | 1.01109 |
| D | 3501.78 | $4.72041 \times 10^{-1}$ | $4.54660 \times 10^{-1}$ | 0.96318 |
| E | 35017.8 | $5.92026 \times 10^{-2}$ | $6.15687 \times 10^{-2}$ | 1.03997 |
| F | 350178 | $5.72630 \times 10^{-3}$ | $7.67816 \times 10^{-3}$ | 1.34086 |

Table 2
Test cases A to F for sloshing with $k = 2\pi/l$, $a_0 = 0.0005$ and $l = 0.2$ giving a comparison between the predicted decay constant, $\alpha_p$ and the computed decay constant, $\alpha_c$

| | | Time increment | | |
|---|---|---|---|---|
| | | $\Delta t = 1.57 \times 10^{-2}$ | $\Delta t = 7.83 \times 10^{-3}$ | $\Delta t = 3.13 \times 10^{-3}$ |
| B.C. | Slip | 0.00143657 | 0.000619007 | 0.000151621 |
| | Semi-slip | 0.00209782 | 0.00115888 | 0.000438266 |
| | Semi-noslip | 0.00136618 | 0.000589279 | 0.000140615 |
| | Robin | 0.0013824 | 0.000601962 | 0.000103919 |

Table 3
Time increment error for all boundary condition schemes

| | | Order of Expansion Basis | | |
|---|---|---|---|---|
| | | $P = 1$ | $P = 3$ | $P = 5$ |
| B.C. | Slip | 0.00061962 | $1.50046 \times 10{-6}$ | $1.91429 \times 10^{-7}$ |
| | Semi-slip | 0.00310734 | 0.000724009 | 0.000243374 |
| | Semi-noslip | 0.00164267 | $5.50922 \times 10^{-5}$ | $2.49173 \times 10^{-5}$ |
| | Robin | 0.00314926 | 0.000161948 | 9.75539e-05 |

Table 4
Spectral error for all boundary condition schemes

|       |              | Slip length | |
|-------|--------------|-------------|-------------|
|       |              | $d/32$      | $d/48$      |
| B.C.  | Semi-noslip  | 0.000585786 | 0.000259526 |
|       | Robin        | 0.0005974   | 000269809   |

Table 5
Slip length error convergence for all boundary condition schemes

| Re    | Analytical | $\frac{\text{Slip}}{\text{Analytical}}$ | $\frac{\text{Semi-slip}}{\text{Analytical}}$ | $\frac{\text{Semi-noslip}}{\text{Analytical}}$ | $\frac{\text{Robin}}{\text{Analytical}}$ |
|-------|------------|------|-------|-------|-------|
| 312   | 0.021887   | 0.886 | 1.53 | 1.93 | 2.046 |
| 3123  | 0.0084967  | 0.182 | 0.914 | 0.977 | 0.973 |
| 31231 | 0.0023462  | 0.255 | 1.019 | 0.930 | 0.931 |

Table 6
Analytical and computationally derived decay rates where computational rates are expressed as a ratio over the analytical value.